This is an open access article published under an ACS AuthorChoice License, which permits copying and redistribution of the article or any adaptations for non-commercial purposes.

ACS central science

Research Article

http://pubs.acs.org/journal/acscii

Raman Scattering in Carbon Nanosystems: Solving Polyacetylene

Eric J. Heller,*[,†,‡] Yuan Yang,[‡] and Lucas Kocia[‡]

[†]Department of Physics and [‡]Department of Chemistry and Chemical Biology, Harvard University, Cambridge, Massachusetts 02138, United States

Supporting Information

ABSTRACT: Polyacetylene has been a paradigm conjugated organic conductor since well before other conjugated carbon systems such as nanotubes and graphene became front and center. It is widely acknowledged that Raman spectroscopy of these systems is extremely important to characterize them and understand their internal quantum behavior. Here we show, for the first time, what information the Raman spectrum of polyacetylene contains, by solving the 35-year-old mystery of its spectrum. Our methods have immediate and clear implications for other conjugated carbon systems. By relaxing the nearly universal approximation of ignoring the nuclear coordinate dependence of the transition moment (Condon approximation), we find the reasons for its unusual spectroscopic features. When the Kramers−Heisenberg−Dirac Raman scattering theory is fully applied, incorporating this nuclear coordinate dependence, and also the energy and momentum dependence of the electronic and phonon band structure, then unusual line shapes, growth, and dispersion of the bands are explained and very well matched by theory.

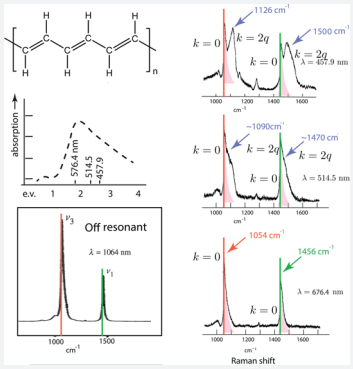

The polyacetylene molecule (Figure 1) once played an outsized role, first as a promising organic conducting polymer,[1] then the focus of the Su−Schrieffer−Heeger[2−4] model for soliton behavior of the Peierls distortion of the chain. Around the same time, intensive work on its spectroscopy, especially Raman spectroscopy, was begun.[5] Heeger, MacDiarmid, and Shirakawa shared the Nobel Prize in Chemistry in 2000 "for the discovery and development of conductive polymers", notably polyacetylene.

The polyacetylene spectroscopy boom trailed off inconclusively. Unusual spectral features were assigned to polydisperse or inhomogeneous samples,[6] unconventional vibrational patterns together with inhomogeneity,[7] and coexistence of ordered and disordered phases (another kind of polydisperse sample).[8] Solitons,[7,8] important as they were for other reasons, were also cited as a cause of the signature Raman scattering effects.

Here, we show that the enigmatic spectral features of polyacetylene, across a wide range of experiments, are in fact attributable to monodisperse samples and Born−Oppenheimer quantum dynamics, especially the transition moments and their coordinate dependence (i.e., no Condon approximation). Molecular ends and internal defects do play a role in the intensity and bandwidth of Raman sidebands, but not their frequencies. The molecule and methods here strongly inform the burgeoning field of Raman spectroscopy of conjugated carbon systems including nanotubes and graphene.

Today, graphene is the new polyacetylene, so to speak. Strong scientific, programmatic, and historical analogies exist between the two systems, including an enigmatic Raman spectrum and hopes for new devices based on conjugated conducting organic crystals. It therefore struck us as odd that polyacetylene's Raman spectrum still remained mysterious, while graphene has enjoyed a well established narrative, for the past 12 years.[11,12]

In Figure 1 we provide an overview of the systems and properties to be understood. As the incident laser energy increases starting from the deep red, the polyacetylene Raman bands evolve gradually from narrow, slightly asymmetric single peaks into a two-peak band consisting of an unshifted sharp peak at lower Raman displacement, tailing off to higher displacement, and a partially overlapping upward shifted sideband peak that becomes dominant in several circumstances.

Making Full Use of the Transition Moment. The key to decoding this rather strange polyacetylene Raman spectrum relies on closely adhering to the well established Kramers−Heisenberg−Dirac (KHD) theory, including the long neglected (in condensed matter theory) nuclear coordinate dependence of the transition moment $\mu(\xi)$, where ξ represents phonon coordinates. The transition moment $\mu(\xi)$ controls the amplitude to absorb a photon as a function of nuclear geometry, i.e., atomic positions defined by the phonon coordinates ξ, and is an integral part of KHD theory (see below). Neglecting the coordinate dependence (called the Condon approximation) is common almost to the point of universal, but we now believe this is quite dangerous, at least in systems consisting of large networks of conjugated carbon. This was recently emphasized by Duque et al., who found that transition moment coordinate dependence was needed to explain spectroscopic data for carbon nanotubes.[13]

No Change in Potential upon Photo Absorption. Because of the dilution of the delocalized π orbital amplitude over the infinite chain, it is almost obvious that the Born−

Received: January 17, 2015
Published: March 23, 2015

 © 2015 American Chemical Society

DOI: 10.1021/acscentsci.5b00021
ACS Cent. Sci. 2015, 1, 40−49

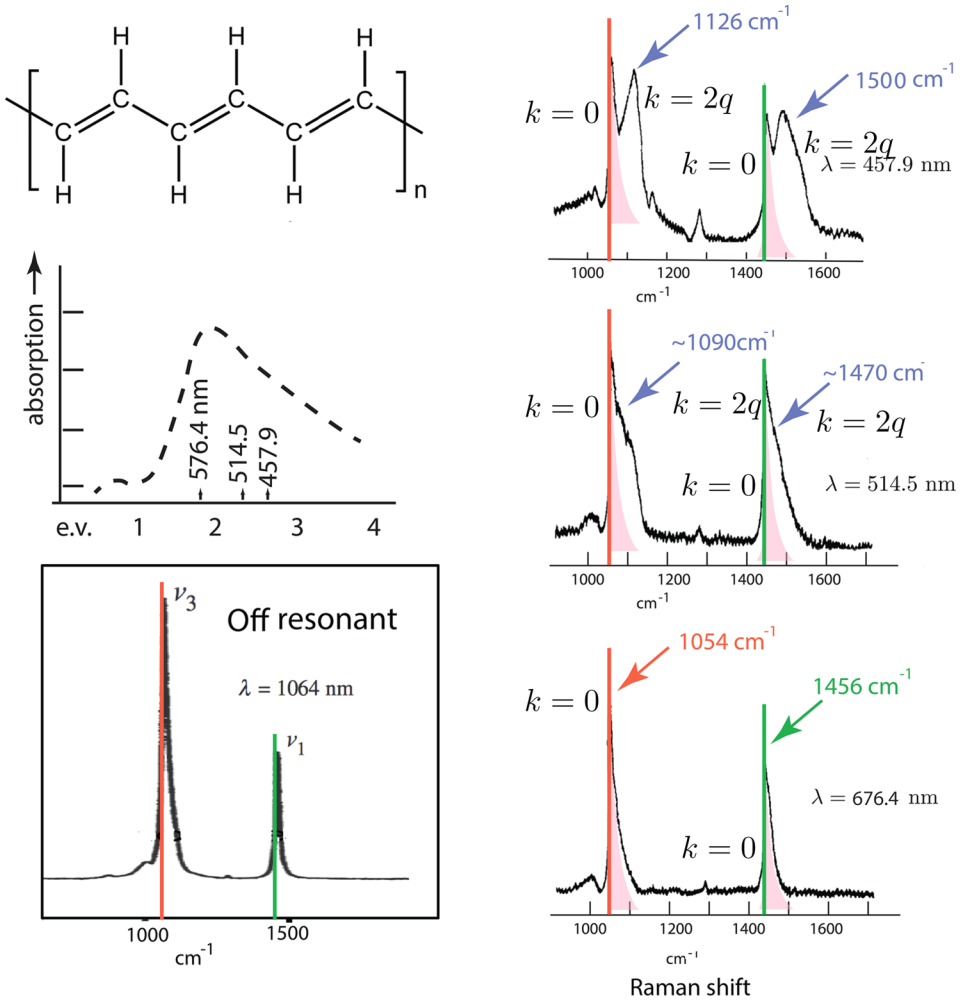

Figure 1. Overview of all-*trans* polyacetylene and its unusual spectroscopy. (Top left) The structure of polyacetylene, with alternating single and double bonds, the result of a Peierls instability. The double bonds are shorter (1.345 Å as against 1.415 Å) for the single bonds, although the π electrons are delocalized over the whole molecule. (Middle left) Absorption spectrum of polyacetylene in the region investigated for resonance Raman scattering. (Bottom left): Off-resonance Raman spectrum of polyacetylene from Gussoni et al.[9] (Copyright 1991 Wiley). (Right column) Some of the major features and changes as incident wavelength decreases, needing an explanation, from 576.4, 524.5, and 457.8 nm. Red and green arrows point to sharp, nearly one-sided bands (shaded pink, tailing off to the right) that show no dispersion (see vertical lines) or growth with incident λ. Blue arrows point to dispersive bands growing in strength and also developing increasing frequency displacement from neighboring $k = 0$ fixed bands (dispersion) with increasing photon energy. Spectral data on the right and middle left are redrawn from Lefrant[10] (Copyright 1983 EDP Sciences).

Oppenheimer potential energy surface is unchanged after a lone electron−hole pair excitation in a large system with a huge number of delocalized orbitals. (Longer times, too long to matter to Raman scattering, can lead to spontaneous localization taking place.[14]) The stability of the Born−Oppenheimer potential against electron−hole pair formation was discussed by Zade[15] et al. where the reorganization energy (the potential energy available in the excited state starting at the ground state geometry) vanished in long linear oligothiophenes with polymer length N. This implies phonons can be created only through the transition moment coordinate dependence $\mu(\xi)$, since no change happens in the potential energy surface. Transition moments and their coordinate dependence are the only active mechanism for phonon production in such systems, within Born−Oppenheimer theory. Transition moment coordinate dependence is a certainty: without it, the polarizability of the system would vanish within Born−Oppenheimer theory.

Of course, in a finite length molecule with defects it is expected that some displacements will occur in the excited states relative to the ground state, even at short times. (We are not interested in longer times beyond where Raman scattering is important.) It is worth noting that intensities created by excited state coordinate displacements are instantaneous in the same sense as the transition moment effects, and are also far from being electron−phonon "scattering". In other words, the populations of the phonons are instantly created, whether it is a transition moment or wave function displacement in the excited state that causes it.

Arriving at Kramers−Heisenberg−Dirac Theory. The underpinnings of the KHD expression[16,17] for Raman scattering, which we use here, are becoming somewhat ragged in the literature. It is not understood in all quarters that the Condon approximation is optional, and in others there is confusion between it and "Franck−Condon theory". Another factor is the popular "double resonance" (DR) Raman theory, associated with a large literature and applied singularly to conjugated carbon compounds like graphene (although not to polyacetylene to our knowledge). DR bears no stated relation

DOI: 10.1021/acscentsci.5b00021
ACS Cent. Sci. 2015, 1, 40−49

to KHD. We could not find the otherwise universally employed KHD Raman theory mentioned anywhere in the extensive double resonance Raman literature, so to clarify matters we derive KHD in a few steps from the same starting point as DR, namely, the Martin and Falicov many-body expression.[18]

The 1925 Kramers–Heisenberg theory for Raman scattering[16] predated quantum mechanics and was based on the Correspondence Principle. Dirac gave the quantum derivation in 1927.[19] The paper by Born and Oppenheimer forming the basis for an intuitive and practical (if approximate) molecular and solid state quantum mechanics came just a bit later (1927).[20] It justified the Franck–Condon principle in terms of the large mass difference between nuclei and electrons. As we will presently see, the KHD expression is fully derivable from the Born–Oppenheimer approximation and light-matter perturbation theory, as is the modern quantum implementation of the Franck–Condon principle.

The Martin and Falicov (MF) many-body expression for general two-photon processes[18] reads

$$\alpha_{2f,1i} = \sum_k \left\{ \frac{\langle \omega_2, f|\mathcal{H}_{\mathrm{MR}}|0, k\rangle\langle 0, k|\mathcal{H}_{\mathrm{MR}}|\omega, i\rangle}{(\hbar\omega - E_k)} \right\} \tag{1}$$

where $\alpha_{2f,1i}$ is an amplitude whose absolute square is proportional to the Raman scattering cross section, with ω_2 the emitted light frequency, ω the incident frequency. The symbols i, k, and f represent initial, intermediate (excited, with energies E_k), and final system eigenfunctions of the full many-body Hamiltonian. $\mathcal{H}_{\mathrm{MR}}$ is the operator controlling the first-order perturbative matter–radiation coupling. The symbol 0 in the intermediate states implies the absence of a photon. We have dropped a second term in the MF expression that corresponds to emission of the photon ω_2 before absorption of the incident photon ω. Unfortunately the full many-body evaluation of the MF expression is far out of reach for systems of interest, and even if it were available, it would be oddly unsatisfying as a pure number lacking physical interpretation or intuition.

It is straightforward to derive the KHD expression by making Born–Oppenheimer approximations to the quantities in the Martin and Falicov expression. We suppress the photon labels since they are implied by the energy differences of the initial and final states; however, the incident frequency still appears in the denominator.

$$|\omega, i\rangle \xrightarrow{\text{Born-Oppenheimer}} |\psi_i(\boldsymbol{\xi}; \boldsymbol{r})\chi_{i,n}(\boldsymbol{\xi})\rangle \tag{2}$$

$$H \xrightarrow{\text{Born-Oppenheimer}} H^{\mathrm{B.O.}} \tag{3}$$

$H^{\mathrm{B.O.}}$ regards the Born–Oppenheimer wave functions $\psi_i(\xi;\boldsymbol{r})$-$\chi_{i,n}(\boldsymbol{\xi})$ as eigenstates with energies $E_{i,n}$. The coordinates $\boldsymbol{\xi}$ represent all the nuclear position or phonon displacements, and $\psi_i(\boldsymbol{\xi};\boldsymbol{r})$ is the usual adiabatic Born–Oppenheimer solution of the ith electronic state, a function of the electron coordinates $\boldsymbol{r}$ for fixed nuclear position $\boldsymbol{\xi}$. The wave function $\chi_{i,n}(\boldsymbol{\xi})$ is the nth vibrational (phonon) state in the ith electronic state. The MF expression becomes

$$\alpha_{fm,i0}^{\rho,\sigma} = \sum_{j,n} \left\{ \left[\langle \psi_f(\boldsymbol{\xi}; \boldsymbol{r})\chi_{f,m}(\boldsymbol{\xi})|\hat{e}_\rho\cdot\boldsymbol{r}|\psi_j(\boldsymbol{\xi}; \boldsymbol{r})\chi_{j,n}(\boldsymbol{\xi})\rangle \langle \psi_j(\boldsymbol{\xi}; \boldsymbol{r})\chi_{j,n}(\boldsymbol{\xi})|\hat{e}_\sigma\cdot\boldsymbol{r}|\psi_i(\boldsymbol{\xi}; \boldsymbol{r})\chi_{i,0}(\boldsymbol{\xi})\rangle \right] / \left[(\hbar\omega + E_{i,0} - E_{j,n}) \right] \right\} \tag{4}$$

where ρ,σ indicate initial and final polarizations of the light. Introducing the transition dipole operator $\mu_{ji}^{\rho}(\boldsymbol{\xi})$,

$$\mu_{ji}^{\rho}(\boldsymbol{\xi}) = \langle \psi_j(\boldsymbol{\xi}; \boldsymbol{r})|\hat{e}_\rho\cdot\boldsymbol{r}|\psi_i(\boldsymbol{\xi}; \boldsymbol{r})\rangle_{\boldsymbol{r}} \tag{5}$$

where the subscript $\boldsymbol{r}$ reminds us that only the electron coordinates are integrated over, we have

$$\alpha_{fm,i0}^{\rho,\sigma} = \sum_{j,n} \left\{ \frac{\langle \chi_{f,m}(\boldsymbol{\xi})|\mu_{fj}^{\rho}(\boldsymbol{\xi})|\chi_{j,n}(\boldsymbol{\xi})\rangle\langle \chi_{j,n}(\boldsymbol{\xi})|\mu_{ji}^{\sigma}(\boldsymbol{\xi})|\chi_{i,0}(\boldsymbol{\xi})\rangle}{(\hbar\omega + E_{i,0} - E_{j,n})} \right\} \tag{6}$$

This is the KHD expression, shown here to be purely the Born–Oppenheimer approximation plus ordinary light-matter perturbation theory. There is a subtle point which needs to be made now: the KHD expression, although a result of light matter perturbation theory, is to be evaluated to give "the answer". That is, it is summed and a number is obtained and that is the Raman amplitude seen in the experiment in a very many cases. Although it is clear that some terms with the vanishing denominators are in a sense "more important" than others, they all count, and they are all to be summed up to get the answer.

The same is true for what can be called the Franck–Condon expression (the quantum embodiment of the Franck–Condon Principle), which is also purely the Born–Oppenheimer approximation plus ordinary light-matter perturbation theory for one photon absorption and emission. It predicts spectral intensities proportional to

$$I_{fm,in}^{\rho} \propto |\langle \chi_{f,m}(\boldsymbol{\xi})|\mu_{fi}^{\rho}(\boldsymbol{\xi})|\chi_{i,n}(\boldsymbol{\xi})\rangle|^2 \tag{7}$$

In both the Franck–Condon and KHD expressions, the Condon approximation means neglect of the coordinate dependence of $\mu_{fi}^{\rho}(\boldsymbol{\xi})$.

Off Resonance: Polarizability and Transition Moments. It is well-known that off-resonance Raman scattering depends primarily on the nuclear derivatives of the Placzek polarizability.[21] Coordinate dependence of the transition moments are responsible for the Placzek polarizability,[17] which would be unacceptably zero in the Condon approximation. Off resonance Raman scattering is necessarily a short time process (due to time-energy restrictions - tuning ΔE below resonance implies at most time $t = \hbar/\Delta E$ allowed in the excited state before re-emission[22]). This gives precious little time for excited state wave function evolution, Born–Oppenheimer or not. Even if atomic displacements were significant (and we have argued that they are not), or if electron–phonon scattering was thought to be important on resonance, phonon production depends increasingly on the static coordinate dependence of the transition moment for Raman intensities as one goes further off resonance. It is an "instant" phonon production process which does not get erased on re-emission, explaining why it dominates off resonance. Coordinate displacements in the excited state can be "erased" upon fast re-emission because there has been insufficient time for wave packet motion under the new regime of excited state

DOI: 10.1021/acscentsci.5b00021
ACS Cent. Sci. 2015, 1, 40–49

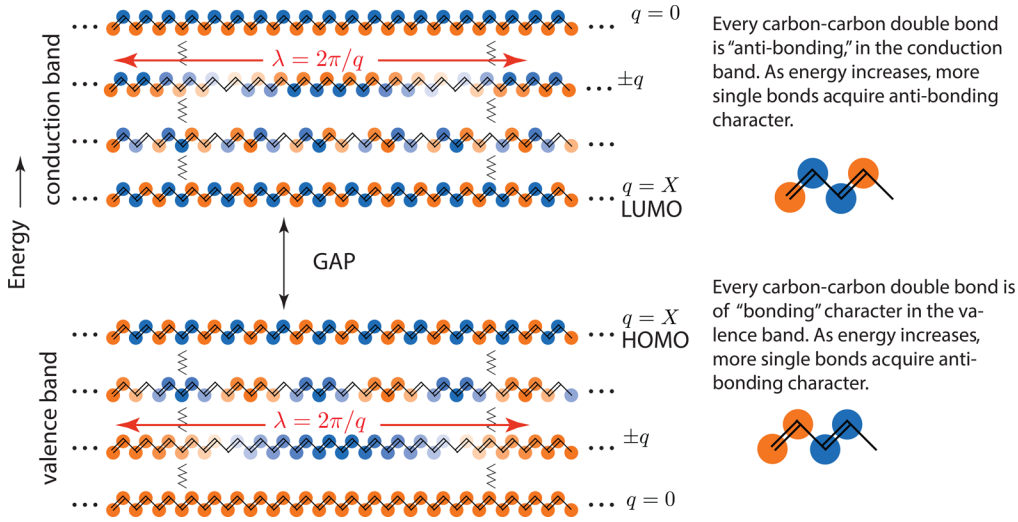

Figure 2. Schematic of the π orbitals in an infinite polyacetylene chain. Each colored dot represents the top half of a carbon p_z orbital, with color giving the sign of that lobe of the orbital. The hidden lobe of each orbital in this top down view is below the plane of the molecule and of opposite sign to the visible part. Transparency depicts wave function amplitude. In the valence band, all double bonds are of bonding character (same sign on adjacent carbons). In the conduction band, all double bonds are of antibonding character.

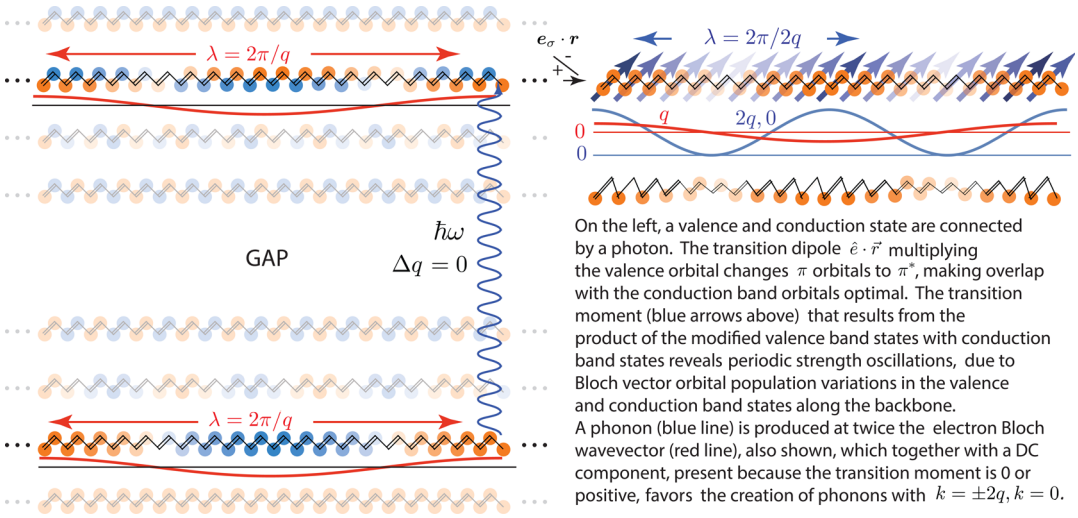

Figure 3. Schematic of transition moment calculation and implications. A photon (blue vertical arrow) creates an electron−hole pair, promoting an electron in a valence orbital to a conduction orbital, here of the same q, conserving crystal momentum (or of opposite q, also conserving crystal momentum and having the same energy, if the birth is accompanied by a creation of a phonon of wave vector $2q$ via coordinate dependence of the transition moment). The phonon energy is prepaid so to speak by reducing the energy of the electronic transition, leaving an energy matched electron and hole from the beginning, $\hbar\omega = \Delta E_{\text{electron transition}} + \Delta E_{\text{phonon creation}}$. The local moments are summed to give the total transition moment and are seen on the right to be modulated *at twice the wavevector of the electronic q*, along the backbone of the molecule. The $2q$ modulation in the transition moment, shown with short blue arrows, going like $M \cos^2(qx) = M/2\,[1 + \cos(2qx)]$ is caused by the oscillation in orbital occupation with Bloch vector q. The strength of M depends on carbon−carbon distances through phonon derivatives $\partial^2\mu^\sigma_{-qq}(\boldsymbol{\xi})/\partial\xi^2_{2q}$; this $k = 2q$ phonon oscillates in-phase with the transition moment, enhancing it at its maxima and doing less diminishment at its minima. Since q changes with photon $\hbar\omega$ according to the electronic band structure, the resulting Raman $k = 2q$ sidebands will show dispersion with incident light frequency. There is also seen to be a constant or "DC" component, corresponding to the q-independent term in the expansion of $\cos^2(qx)$; this creates a Γ-point $k = 0$ phonon and band, independent of the excitation frequency or q, i.e., with no dispersion.

forces, implying a return to the initial phonon state upon re-emission, with high probability.

Accounting for Energy and Pseudomomentum. The electron energy adjustment due to instantaneous phonon production is evident in eq 6 since the largest terms correspond to a vanishing $(\hbar\omega + E_{i,0} - E_{j,n})$, i.e., when the excited electronic energy plus the phonon energy, $E_{j,n}$, equals the initial energy in the system $E_{i,0}$ plus the photon energy $\hbar\omega$. We remark here that normally a small imaginary part is added to the dominator, so that a range of terms, not one term, dominates. This imaginary part represents spontaneous radiation rates, for example, but it can effectively be quite a bit larger if there are missing degrees of freedom not accounted for, such as a bath of particles interacting with the system. Therefore, in spite of the appearance of the sum, it is not normal for one term to dominate it even at special frequencies ω. The exception to this is small molecules, with discrete levels in the excited state; we are not concerned with this here. Nonetheless, with a small imaginary part, the most important terms still have very nearly perfect energy compensation built-

DOI: 10.1021/acscentsci.5b00021
ACS Cent. Sci. 2015, 1, 40−49

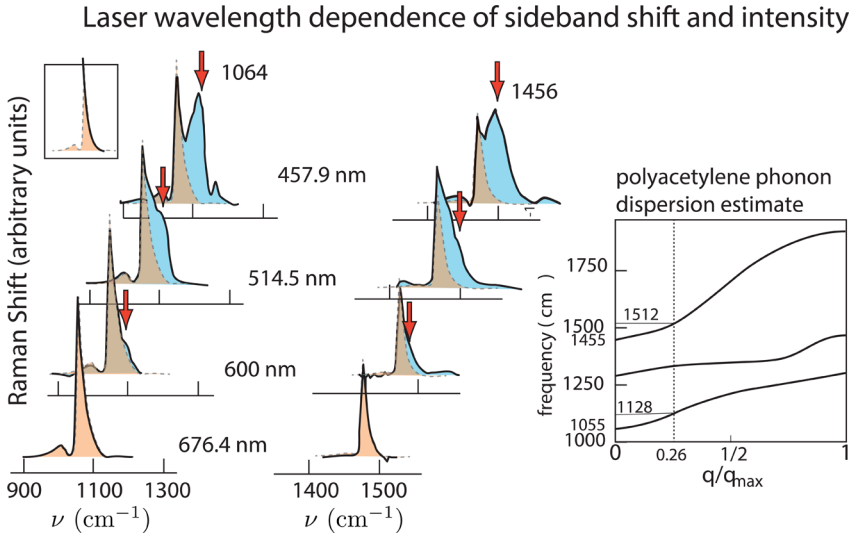

Figure 4. Dispersion and growth of the 1064 and 1456 cm^{-1} sidebands of *trans*-polyacetylene taken by Mulazzi et al. at the laser frequencies shown, redrawn from ref 6 (Copyright 1983 Elsevier). Our prediction of sideband position, using the phonon bands in the inset, right, is shown by the red arrows. (We have not found a well established, "most reliable" phonon dispersion for polyacetylene.) One can alternately say we have here established the phonon dispersion in the early part of the bands for the first time, through interpretation of the experiments. The overall line shape is the sum of the constant $k = 0$ band and the moving and growing $k = 2q$ sideband. The inset (upper left) shows the $k = 0$ band fit to an exponential falloff on the right for the 1064 cm^{-1} band. Inset, right: Polyacetylene phonon dispersion curves according to Jumaeu et.al.,[23] used here.

in; that is, the electronic transition energy is adjusted downward at the get-go to compensate for the creation of phonons. It is also adjusted upward for annihilation of phonons, which can result in anti-Stokes scattering.

Tight Binding Model. We present a polyacetylene tight binding model using out of plane carbon p_z orbitals. The model provides the basis for the derivations to follow. Figures 2 and 3 show a top-down representation of a portion of an infinite length quasi-1D polyacetylene crystal. The lowest and highest extremal $q = 0$ (crystal momentum zero) Γ point states and representative intermediate states for the valence and conduction bands are shown. The valence band electronic states exclusively consist of bonding π orbitals (same sign on both carbon atoms) on the double bonded carbons, and the conduction bands exclusively consist of antibonding π orbitals (opposite sign) on the double bonded carbons.

The figures and their captions make clear that $k = 0$ fixed and $k = 2q$ oscillating transition moment densities result, where q is the Bloch wave vector of the conduction band electronic orbital created by the incoming photon. The tendency for the transition moment to change with phonon Bloch vector k will depend on whether it is in-phase with the transition momentum oscillations. It will clearly have a maximum at the $2q$ transition density oscillation wave vector, causing phonons to be produced at $k = 2q$, and more to be produced at $k = 0$, caused by the constant part of the transition density. The $k = 0$ phonon creation involves no momentum change for the electron. The transition will have been made at lower energy to account for the phonon energy as described above and therefore produces a perfectly matched electron and hole. The $k = 2q$ phonon on the other hand will have given a backward kick to the electron, taking it from q to $-q$, so the electron needs elastic backscattering $k = 2q$ to realign it with the hole, allowing Raman emission and thereby sideband intensity.

The cause of the sideband dispersion is already clear, namely, the electronic band structure, with q changing as photon and thus electron energy changes, and the $2q$ phonon reacting with an appropriate photonic band structure energy shift (see Figure 4, right). It is clear that sources of backscattering such as defects and molecular termination will facilitate electron−hole annihilation and increase sideband intensity. Already this simple model reveals the essence of striking sideband variations in frequency and intensity as laser frequency changes, and as backscattering is made more or less prevalent.

The valence band Born−Oppenheimer electronic orbital $\psi_{q^v}(\boldsymbol{\xi};\ \boldsymbol{r})$ possesses Bloch vector q^v (reducing to one-dimensional notation in the pseudo 1D crystal). It depends on phonon coordinates $\boldsymbol{\xi}$, and electron coordinates $\boldsymbol{r}$. The available conduction band state $\psi_{q^c}(\boldsymbol{\xi};\ \boldsymbol{r})$ has the same Bloch vector (in the case of the $k = 0$ band, or a reversed Bloch vector $-q$ if a term in the transition moment creates a phonon of wavevector $k = 2q$). We will see why these processes turn up as Raman scattering below. We say right now that according to our model, there are plenty of other processes going on starting in the excited state that do not show up as Raman scattering.

Specializing eq 5 to the present case of a linear periodic system, the transition moment for polarization $\hat{\boldsymbol{e}}_\sigma$ and electron pseudomomentum q^v and q^c in the valence and conduction bands, respectively, is written according to eq 5 above

$$\mu^{\sigma}_{q^c q^v}(\boldsymbol{\xi}) = \langle \psi_{q^c}(\boldsymbol{\xi};\ \boldsymbol{r}) | \boldsymbol{e}_\sigma \cdot \boldsymbol{r} | \psi_{q^v}(\boldsymbol{\xi};\ \boldsymbol{r}) \rangle_{\boldsymbol{r}} \tag{8}$$

We proceed to make this more specific to see how the "suggestive" tight binding model given earlier can be used explicitly to give the selection rules observed in the experimental spectrum. The tight-binding wave functions can be expanded

$$\psi_{q^v}(\boldsymbol{\xi};\ \boldsymbol{r}) = \sum_n e^{iq^v \cdot \boldsymbol{R}_n(\boldsymbol{\xi})} \phi(\boldsymbol{r} - \boldsymbol{R}_n(\boldsymbol{\xi})) \tag{9}$$

where ϕ is a p_z orbital and where the atomic coordinates $\boldsymbol{R}_n(\boldsymbol{\xi})$ depend here explicitly on the phonon coordinates $\boldsymbol{\xi}$. After this tight binding form (and one like it for the conduction band) is inserted into the expression eq 8 for the dipole transition

DOI: 10.1021/acscentsci.5b00021
ACS Cent. Sci. 2015, 1, 40−49

moment, using the velocity (derivative) form of the dipole operator, noting the vanishing diagonal terms $\int \mathrm{d}r\ \phi(\boldsymbol{r} - \boldsymbol{R}_n(\boldsymbol{\xi}))(\mathrm{d}/\mathrm{d}\boldsymbol{r})\ [\phi(\boldsymbol{r} - \boldsymbol{R}_n(\boldsymbol{\xi}))] = 0$, and keeping only the nearest neighbor off diagonal terms, we obtain

$$\mu^{\sigma}_{q^c q^v}(\boldsymbol{\xi}) \propto \sum_n e^{-i(q^c - q^v)\cdot \boldsymbol{R}_n(\boldsymbol{\xi})}\ \{e^{iq^v\cdot\Delta_{n-1,n}(\boldsymbol{\xi})} D^{\sigma}_{n-1,n}[|\Delta_{n-1,n}(\boldsymbol{\xi})|] + \mathrm{e}^{-iq^v\cdot\Delta_{n,n+1}(\boldsymbol{\xi})} D^{\sigma}_{n,n+1}[|\Delta_{n,n+1}(\boldsymbol{\xi})|]\}, \tag{10}$$

where

$$\Delta_{n-1,n}(\boldsymbol{\xi}) = \boldsymbol{R}_{n-1}(\boldsymbol{\xi}) - \boldsymbol{R}_n(\boldsymbol{\xi});$$
$$\Delta_{n,n+1}(\boldsymbol{\xi}) = \boldsymbol{R}_n(\boldsymbol{\xi}) - \boldsymbol{R}_{n+1}(\boldsymbol{\xi}) \tag{11}$$

The factor $D^{\sigma}_{n-1,n}\ [|\boldsymbol{\Delta}_{n-1,n}(\boldsymbol{\xi})|]$ and its partner $D^{\sigma}_{n,n+1}$ one site away are the dipole matrix elements

$$D^{\sigma}_{n-1,n}[|\Delta_{n-1,n}(\boldsymbol{\xi})|] = \int \mathrm{d}\boldsymbol{r}\ \phi(\boldsymbol{r} - \boldsymbol{R}_{n-1}(\boldsymbol{\xi}))\ \boldsymbol{e}_{\sigma}\cdot(\mathrm{d}/\mathrm{d}\boldsymbol{r})\ [\phi(\boldsymbol{r} - \boldsymbol{R}_n(\boldsymbol{\xi}))] \tag{12}$$

between neighboring π orbitals; these are quite clearly dependent on the distance between the adjacent carbon atoms.

It is crucial that unless atom−atom distance derivatives like $\partial\boldsymbol{\Delta}_{n-1,n}(\boldsymbol{\xi})/\partial\xi_k$ for certain ξ_k vary in a synchronized way with the Bloch factor $e^{i(q^c - q^v)\cdot\boldsymbol{R}_n(\boldsymbol{\xi})}$, the dipole moment derivatives like

$$\frac{\partial\mu^{\sigma}_{q^c q^v}(\boldsymbol{\xi})}{\partial\xi_k} \tag{13}$$

will vanish, along with any chance of creating a phonon in coordinate ξ_k of momentum k. But the phonons have a variety of pseudomomenta, and for many combinations of q^c and q^v several may be available to "neutralize" the phase drift of the term $e^{i(q^c - q^v)\cdot\boldsymbol{R}_n(\boldsymbol{\xi})}$. The exponent acquires a net term

$$e^{i(q^c - q^v - k)\cdot\boldsymbol{R}_n(\boldsymbol{\xi}_0)} \tag{14}$$

and the sum over n along an infinite chain will vanish as promised unless $q^c - q^v - k = 0$.

The first nonvanishing possibilities that present themselves are $q^c = q^v$ and $k = 0$ (associated with a Γ point phonon $\xi_{k=0}$), and $-q^c = q^v$ together with $k = 2q$ (dropping the valence-conduction labels). This is associated with a sideband phonon $k = 2q$. Whereas the Γ point phonon is immediately able to recombine with its hole emptied in the valence band (the electron and hole are exactly matched), the sideband electron can reunite with the hole only after elastic backscattering, when again it becomes perfectly matched, and if it emits it reveals the presence of the phonon, which is present in any case.

However, many other phonons can be produced with a variety of electron valence and conduction pseudomomenta such that $q^c - q^v - k = 0$, which sounds like a problem: too many phonons! However, there is an efficient gatekeeper normally preventing Raman emission from such phonons, even though they are present: Pauli blocking prevents such unmatched electrons and holes, $|q^c| \neq |q^v|$ from recombining even after elastic backscattering. What makes the gatekeeper so strict is that time is very short, and there is no time to get "sloppy" about electron−hole matching: e-e scattering is utterly destroying the memory of conditions of the conduction electron on a time scale of femtoseconds.

Given the requirements of pseudomomentum matching upon photo absorption in infinite periodic systems, both the hole and the particle equally share the adjustment of their energy to "pay" for the birth of the phonon. Suppose the ground state electron pseudomomentum is q with a quiescent phonon bath. In the excited state, phonons with a range of k's are born; the transition moment is indiscriminate about this. Among these are phonons with momentum $2q$, causing the electron to be born at $-q$ instead of q by momentum conservation. Elastic backscattering $k = 2q$ then perfectly realigns the electron with its hole. Phonons born instead at arbitrary k can be backscattered or not, but unless $k = 2q$ a moment's thought reveals the result is a stillborn, i.e., a Pauli blocked electron. This implies many unused incoming photons generate phonons not seen in Raman spectra. Let us remind ourselves that the total yield of Raman photons is often on the order of one in 10 million incoming photons, much less in a given band. This explains the special appearance of pseudomomentum $2q$. It is characteristic of the sideband dispersion and permitted (free of) Pauli blocking.

The Kramers−Heisenberg−Dirac expression, eq 6, with minor notational adjustment appropriate to polyacetylene, scattering from the initial valence electronic state with Bloch vector q with no phonons present, i.e., $|\chi_0(\boldsymbol{\xi})\rangle$, to conduction states at q (or $-q$ if a phonon with pseudomomentum $2q$ has been created in the jth phonon band), finally (after backscattering if necessary) emitting back to the ground electronic state into phonon wave function $|\chi_{j,2q}(\boldsymbol{\xi})\rangle$ following electron−hole recombination, reads

$$\hat{\alpha}^{\sigma\rho}_{v,j,k;v,0} = \sum_{c,j',k'} \Big\{\Big(\langle\chi_{j,2q}(\boldsymbol{\xi})\rangle|\mu^{\sigma}_{q^v q^c}(\boldsymbol{\xi})|\chi_{j',k'}(\boldsymbol{\xi})\rangle \langle\chi_{j',k'}(\boldsymbol{\xi})\rangle|\mu^{\rho}_{q^c q^v}(\boldsymbol{\xi})|\chi_0(\boldsymbol{\xi})\rangle\Big) / \Big(\hbar\omega + E_{v,0} - E_{c,j,k}\Big)\Big\} \tag{15}$$

where $E_{c,j,k}$ is the energy of the phonon of wave vector k in band j and electronic conduction band c. The initial state $|\chi_0(\boldsymbol{\xi})\rangle$is multiplied by the transition moment $\mu^{\sigma}_{q^v q^c}(\boldsymbol{\xi})$, producing

$$\mu^{\rho}_{q^c q^v}(\boldsymbol{\xi})|\chi_0(\boldsymbol{\xi})\rangle = \left(\mu^{\rho}_{q^c q^v}(\boldsymbol{\xi}_0) + \sum_{j,k} \left.\frac{\partial\mu^{\rho}_{q^c q^v}(\boldsymbol{\xi})}{\partial\xi_{j,k}}\right|_{\boldsymbol{\xi}_0} \cdot\xi_{j,k} + \ldots\right)|\chi_0(\boldsymbol{\xi})\rangle \tag{16}$$

where the subscripts j, k on ξ refer to wave vector kth in the jth phonon band. This implies *instant phonon creation*, since

$$\mu^{\rho}_{q^c q^v}(\boldsymbol{\xi})|\chi_0(\boldsymbol{\xi})\rangle = \mu^{\rho}_{q^c q^v}(\boldsymbol{\xi}_0)|\chi_0(\boldsymbol{\xi})\rangle + \sum_{j,k}\left(\frac{\partial\mu^{\rho}_{q^c q^v}}{\partial\xi_{j,k}}\right)\cdot\xi_{j,k}|\chi_0(\boldsymbol{\xi})\rangle + \frac{1}{2}\sum_{j,k;j'k'}\left(\frac{\partial^2\mu^{\rho}_{q^c q^v}}{\partial\xi_{j,k}\partial\xi_{j',k'}}\right)\cdot \xi_{j,k}\xi_{j',k'}\ |\chi_0(\boldsymbol{\xi})\rangle + \cdots = a^{\rho}_0|0\rangle + \sum_{j,k} b^{\rho}_{j_k}|k_j\rangle + \sum_{j,k;j',k'} c^{\rho}_{k_j;k'_{j'}}\ |k_j, k'_{j'}\rangle + \cdots \tag{17}$$

after rewriting the polynomials multiplying the ground state in terms of the equivalent set of excited phonon modes. This is a sum over the ground and excited conduction band phonon

DOI: 10.1021/acscentsci.5b00021
ACS Cent. Sci. 2015, 1, 40−49

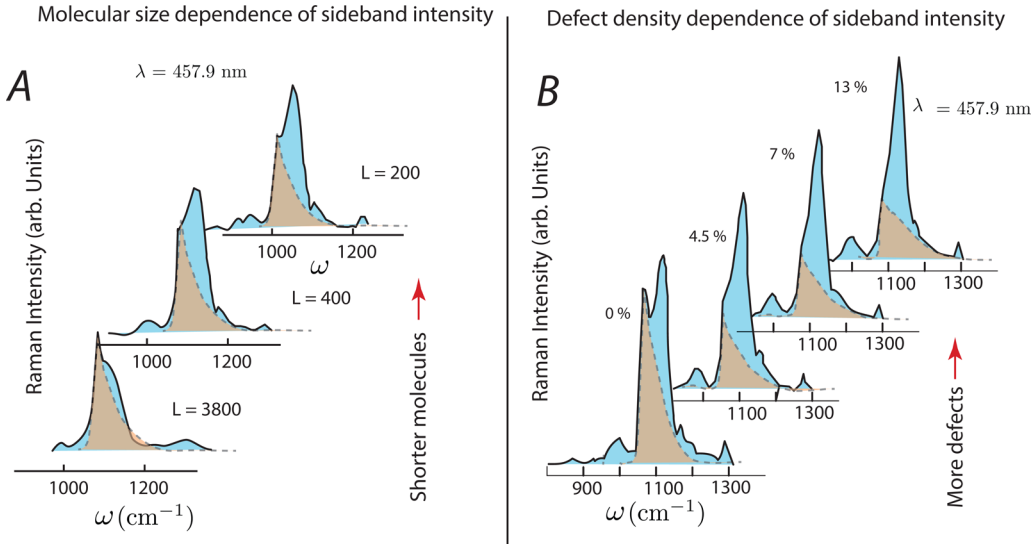

Figure 5. Dispersion and growth of Raman sidebands with length and defects. (A) As the polyacetylene length becomes shorter in a monodisperse sample, the ends of the molecule become accessible to a higher fraction of the electrons, increasing the backscattering efficiency. The $k = 2d$ intensity *falls* like the inverse length of the molecule. The figure was redrawn and the dashed $k = 0$ band contribution added, from ref 24 (Copyright 1988 American Institute of Physics). (B) As the density of defects increases, the $k = 2q$ dispersive sideband accounts for an increasing fraction of the Raman scattering in the 1054 cm^{-1} band. Other sideband features in different bands show the same behavior. The figure was redrawn and the dashed $k = 0$ band contribution added, starting from Schäfer-Siebert et al.[25] (Copyright 1987 Elsevier). Important details: (1) the sideband increases intensity but does not broaden in fwhm after 4.5% defects. The sideband width and line shape are not determined by the time it takes to backscatter. (2) The $k = 0$ band is added to the sideband to give the total intensity, making a break in slope of the total to the right of the $k = 0$ band peak in both A and B panels (and verified in the numerical calculations, Figure 6).

modes with Bloch wavevectors $|k_j\rangle$, $|k_j,k'_{j'}\rangle$, ..., including possible multiple occupation different bands j and j' of different or the same wavevector k_j and k'_j in the electronic band q, of which here we consider two, the π valence and conduction bands.

Transition Moment Estimates. There is indeed a strong dependence of the propensity to make a π to π^* transition depending on carbon−carbon interatomic distance, in a single bond. However, does this survive the transformation to a finite derivative with respect to phonon coordinates in the long molecule limit? Detailed arguments given in the Supporting Information show this is the case, but there is a very quick and convincing shortcut to the conclusion: if the phonon coordinate derivatives vanished, the off resonance Raman scattering the phonon modes in question would too. This is obviously not the case (see Figure 1). The Placzek polarizability derivatives[17] used for calculating off-resonant Raman scattering[21] depend on these derivatives.

A simple estimate of the transition moments and their coordinate dependence for polyacetylene along, for example, the C═C double bond direction may be had using tight binding and Gaussian orbitals. In arbitrary units, we find transition moments (constant term) near 25, and the first derivative along a C═C stretch 1456 cm^{-1} phonon mode of about 16 per angstrom of double bond stretch. The individual C═C dimer stretch is however diluted roughly by $1/(N)^{1/2}$ in a phonon mode, where N is the number of dimer units along the chain. The Raman intensity to the phonon goes as the square of this, or $1/N$. There is another factor of $1/N$ diluting the transition moment, coming from the average $1/(N)^{1/2}$ reduction of the orbital amplitude on each bond, keeping the delocalized electronic orbitals of a given q normalized. The transition moment involves multiplication of two such orbitals on each dimer, but the integral involves integrating over all N dimers. The orbital dilution is thus canceled in the transition moment integral. There still remains the $1/N$ phonon dilution in Raman intensity. However, the full KHD expression involves a sum over all electronic states, resonant or not. It is easily shown, after summing over nearly resonant terms, that the total Raman intensity to a given phonon mode, given a small damping, e.g., including spontaneous radiation), becomes constant as $N \to \infty$. This makes sense, since one electron is making a transition over the whole polymer.

Sideband Dispersion, Backscattering. The Taylor expansions of the coordinate dependence of the transition moment is sometimes called a Herzberg−Teller expansion; it is not a perturbation expansion but merely a way to organize its coordinate dependence. Electronic structure calculations can yield the full coordinate dependence at an *ab initio* level, boding well for future quantitative prediction of Γ point band strengths. Prediction of sideband strength depends on total backscattering, which requires sophisticated understanding of kinks, environment, other defects, and their backscattering amplitudes. This is beyond our current capabilities, but we later show revealing trends with changes that can only increase or decrease backscattering, such as proximity to molecular ends, introduction of defects, etc.

The presence of $k = 2q$ phonons could in principle also backscatter electrons elastically, but experiments (see below) show the $k = 2q$ sideband intensity effectively vanishing if artificial sources of backscattering are absent, so such backscattering is evidently not important. A $k = 2q$ sideband should be attached to every high symmetry point, subject to selection rules, again because of the transition moment undulations, which produce a DC component populating the high symmetry point and another component at $k = 2\ q$.

If a phonon of wave vector $k = 2q$ is created instantaneously upon excitation, the energy devoted to the electronic transition is adjusted by the phonon energy, according to the total energy

DOI: 10.1021/acscentsci.5b00021
ACS Cent. Sci. 2015, 1, 40−49

in the photon: $\hbar\omega = E_{\text{electrontransition}} + E_{\text{phonon}}$. The phonon's energy dispersion is thus written into the photon's Raman sideband dispersion.

The $k = 2q$ phonon sidebands diminish in strength (and move toward the $k = 0$ line as q diminishes) with redder incoming light and are missing altogether below resonance. If the phonons are reliably produced as a byproduct of the transition moment, why do corresponding Raman sidebands diminish in intensity this way? Off resonance, there is insufficient time to backscatter the conduction band recoiling electrons, so they remain very unlikely to find their way back to the hole they left behind. There is no such problem for the $k = 0$ band, since the electron did not change crystal momentum in the first place. These facts contribute to the large change in the ratio of $k = 0$ and $k = 2q$ Raman band intensities with incident frequency. In summary, phonons of both types, sidebands and main peak, are reliably created, but the fraction of sideband that gives rise to Raman shifted emission depends on backscattering conditions.

Absorption vs Emission. The question arises whether the phonon production must occur only in absorption, since the transition moment acts twice, once absorbing a photon and once emitting one. Indeed the $k = 0$ band may be generated in either step or both. The story for the sidebands is different. A sudden exchange $-q$ for q producing a phonon $2q$ upon emission would make recombination unlikely.

Defects and Finite-Sized Molecules. What makes the features of the polyacetylene Raman band shapes peculiar, beyond the dispersion of $k = 2q$ Raman bands, is the strongly variable strength of the (broadened) sidebands depending on conditions, and the width and shape of the band. These are not Gaussian or Lorenzian lineshapes obeying a sum rule! The band shapes and their evolution with incident wavelength can be explained in terms of the different responses of the $k = 0$ peak and the $k = 2q$ peak to the effects of backscattering.

The $k = 0$ Γ point bands are always present for Raman allowed transitions, induced by the constant component of transition moment; these do not require backscattering in order to be produced. The exponential tail to the right of the sharp $k = 0$ feature at 1164 cm^{-1} is found not to depend strongly on backscattering strength (pink and tan shaded regions, Figures 4 and 5).

With modest concentrations of defects and presence of ends, k and q are no longer perfectly good quantum numbers, effectively making k's close to 0 allowed. Defects also play a dual role in the $k = \pm 2q$ sideband, making nearby k's available and backscattering electrons so they can fill the holes they created. The degeneracy of left and right traveling plane waves is broken, both electronically and vibrationally.

The phonons associated with the $k = 0$ line carry no pseudomomentum even as they carry energy above that of the $k = 0$ line. The energies do not lie below the $k = 0$ line because no phonon states exist there, since even with defects present, it is difficult to generate vibrations of lower frequency than the Γ point of each band. Confining the vibrations tends to produce higher, not lower, frequencies if the band dispersion slope is positive, as it is here. Thus, the abrupt falloff to the left of the Γ point line.

Experimental Tests. It is remarkable that three critical experimental tests were performed supporting the transition moment/backscattering model given here: varying the incident wavelength[6] that we have already mentioned, varying the length of the molecule in a controlled way,[24] and varying the defect density in a controlled way.[25]

In ref 24, three samples of nearly monodisperse polyacetylene with lengths of about 200, 400, and 3800 unit cells were synthesized and their Raman spectra were obtained. The sidebands remained, and many of the earlier "polydisperse" explanations for the line shape quickly evaporated.

A shorter polyacetylene molecule has ends available to backscatter to a larger fraction of electrons. The prediction is that the $k = 2q$ sideband intensity falls like the inverse length of the molecule, assuming no defect scattering. The $(k = 0)/(k = 2q)$ ratio in the three parts of Figure 5A using the same $k = 0$ band shape (dashed line) as in Figure 4 changes by a factor of 1:7.5. Assuming a (crude guess) 50 unit cell proximity rule in order to reach the end intact to backscatter, the ratio should have been roughly 1:10. In any case, the experiment clearly shows that accessible ends dramatically enhance the $k = 2q$ band, according to both the model and the experiment (see Figure 5A).

Another key measurement[25] involved controlled oxidation of the polyacetylene (see Figure 5B), resulting in a knowable *additional* defect density (over the nascent density) of 0%, 4.5%, 7%, or 13%, see Figure 5. The ratio of the larger to smallest $(k = 0)/(k = 2q)$ sideband intensity is about 1:6 going from 0% to 13% new defects, meaning six times as many electrons relax by backscattering, emitting, and filling their holes with the highest defect density compared to nascent density plus end effects.

Finally, we discuss the trends with laser frequency,[6] as seen in Figure 4. We have already mentioned that being off resonance eliminates the sidebands, due to a cutoff in the time allowed to backscatter (see Figure 1). Preliminary calculations using 20 unit cells (40 carbon atoms) polyacetylene molecules with defects caused by Si replacing C, or oxidation giving a carbonyl in place of a normal chain carbon, both show a general trend toward increased localization, some of it very severe, of the hole especially as the hole energy is reduced (as happens at higher photon frequency). This trend would support the growth of the sideband area with shorter laser wavelengths, but should be viewed as tentative pending more extensive structure calculations. Another trend may be the growth in the number of possible sideband transitions as dispersion opens a larger gap (on the order of 50 cm^{-1}) between the $k = 0$ and $k = 2\,q$ peaks. More states become available to be populated with phonons. Rayleigh scattering is still by far the dominant process, so there is much leeway for phonon production to become a larger fraction of events following photoabsorption.

Numerical Check. As a check on the mechanisms for line shape evolution, we constructed a tight binding model with the molecular backbone represented by alternating bonds, of length 450 unit cells, including two or four randomly placed 10% mass defects. The spectra were calculated for each case by assuming constant and sinusoidal "driving terms" coming from transition moments of the electronic transitions. The spectrum was computed by calculating the excitability of each phonon mode of the chain at the given driving q's (with impurities in place), and adding its contribution to the Raman shift spectrum at the mode's frequency. The overall sideband backscattering intensity (but not its frequency or line shape or line width) was adjusted to match weak, moderate, and strong backscattering limits. Various limits of high and low impurity, long and short molecules, etc. were investigated this way. The results for various combinations are shown in Figure 6, which should be

DOI: 10.1021/acscentsci.5b00021
ACS Cent. Sci. 2015, 1, 40−49

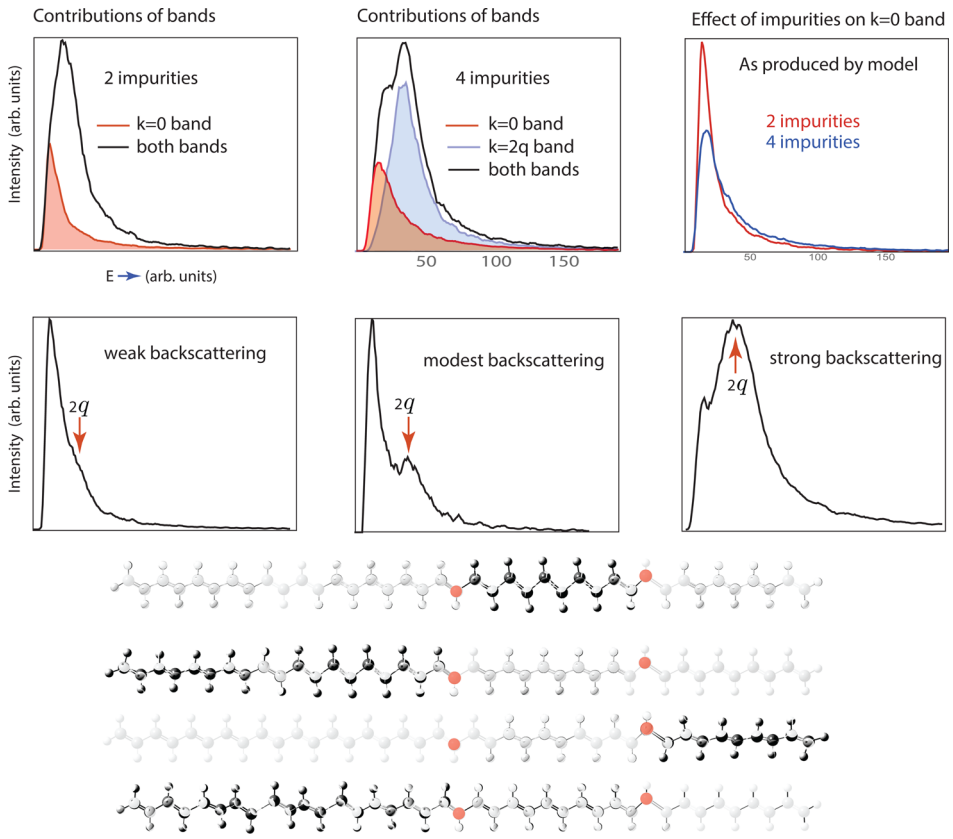

Figure 6. Numerical results from a simple phonon simulation as input to the Raman theory presented in this paper. The calculations involve a 450 unit cell long sample with alternating "bonds" and two or four randomly placed defect impurities. The defective phonons we found by diagonalizing the Hessian matrix of a linear chain of 900 atoms (450 unit cells). About 3000 placements of the random impurities were averaged here for each result shown. The electronic orbitals were assumed to ignore the impurities and span the sample. The $k = 0$ and $k = 2q$ components can be computed separately (see their contribution to the total in the top row), and their ratio varied by hand. It would be difficult in the extreme to get the backscattering intensity *ab initio*, because a quantitative theory giving the number of defects of all sorts, and their backscattering propensities, would be required for samples produced in a given lab. The line shapes nonetheless emerge naturally from the simulation; these are *not* put in by hand so to speak. They are due to the partial vibrational confinement between ends and defects, seen at the bottom in another simulation (a Gaussian 09 density functional calculation on polyacetylene with four Si atoms in place of carbon). Four low lying vibrational modes are seen, with darkness of the atoms representing vibration amplitude. The vibrational modes have a near linear dispersion in this low k regime and are driven by the constant and sinusoidal terms in the transition moment, as in the tight binding model presented above in Figures 2 and 3. See text and Supporting Information for more details on the calculation.

compared with Figures 4, 5, and 1. It takes about 3000 random realizations of the impurity positions before the average (shown) settles down. More details on the calculation, including *Mathematica* code, can be found in the Supporting Information.

■ METHODS

The use of standard quantum chemistry package Gaussian 09 in places was mentioned in the text, and the code for the sideband simulation is available on request in Mathematica format.

■ IMPLICATIONS AND CONCLUSION

The spectrum of polyacetylene has been explained, in terms of Kramer–Heisenberg–Dirac Raman scattering theory, without using the Condon approximation to KHD that treats transition moments as a constant. The key is indeed the transition moment and its coordinate dependence, leading to immediate phonon production upon electron–hole pair formation. This means the phonon energies are subtracted from the electron at birth in the excited state, yielding a q matched electron and hole. In an infinite crystal with delocalized orbitals there is no structural change nor new forces in the excited states, making the transition moment solely responsible for the Raman signal. Electron–phonon scattering plays no role, except to knock out candidate emitters, helping to keep the time scale allowed for Raman emission very short; e-e scattering is thought to be much faster, however.

It is important, if difficult perhaps, to experimentally check for the predicted instant presence of phonons after photo-absorption. Raman emission in the sidebands is delayed waiting for backscattering, but in the $k = 0$ bands is immediate. This means there should be an evolution of the sidebands with time, in a pulsed experiment.

The implications of this work for other conjugated carbon systems, including nanotubes and graphene, are clear: The ideas put forth here carry over immediately and promise new insight into the information that Raman spectroscopy can provide on the "quantum clockwork" of many carbon nanosystems.

■ ASSOCIATED CONTENT

Ⓢ Supporting Information

More information on Herzberg–Teller strength estimates, the numerical simulation, and significant earlier theories of the

DOI: 10.1021/acscentsci.5b00021
ACS Cent. Sci. 2015, 1, 40–49

Raman spectrum of polyacetylene. This material is available free of charge via the Internet at http://pubs.acs.org.

■ AUTHOR INFORMATION

Corresponding Author

*E-mail: heller@physics.harvard.edu.

Notes

The authors declare no competing financial interest.

■ ACKNOWLEDGMENTS

The authors acknowledge support from the NSF Center for Integrated Quantum Materials (CIQM) through Grant NSF-DMR-1231319. We thank the Faculty of Arts and Sciences and the Department of Chemistry and Chemical Biology at Harvard University for generous partial support of this work. We also thank Prof. Philip Kim for helpful conversations. We also sincerely thank two referees for a very careful reading of the manuscript and for providing many helpful suggestions.

■ REFERENCES

(1) Chiang, C.; Fincher, C.; Park, Y.; Heeger, A.; Shirakawa, H.; Louis, E.; Gau, S.; MacDiarmid, A. *Phys. Rev. Lett.* **1977**, *39*, 1098−1101.

(2) Su, W.; Schrieffer, J. R.; Heeger, A. J. *Phys. Rev. Lett.* **1979**, *42*, 1698.

(3) Heeger, A.; Kivelson, S.; Schrieffer, J.; Su, W. *Rev. Mod. Phys.* **1988**, *60*, 781−850.

(4) Bryce, M. R.; Ahmad, M. *Nature* **1984**, *311*, 301−302.

(5) Kuzmany, H. *Phys. Status Solidi B* **1980**, *97*, 521−531.

(6) Mullazzi, E.; Brivio, G. P.; Faulques, E.; Lefrant, S. *Solid State Commun.* **1983**, *46*, 851−855.

(7) Ehrenfreund, E.; Vardeny, Z.; Brafman, O.; Horovitz, B. *Phys. Rev. B* **1987**, *36*, 1535−1553.

(8) Kuzmany, H.; Imhoff, E. A.; Fitchen, D. B.; Sarhangi, A. *Phys. Rev. B* **1982**, *26*, 7109.

(9) Clark, R. J. H.; Hester, R. E. *Spectroscopy of Advanced Materials*; Wiley: New York, 1991; Chapter 5, pp 251−353.

(10) Lefrant, S. *J. de Physique Colloq.* **1983**, *44*, C3-247.

(11) Neto, A. C.; Guinea, F.; Peres, N. M. R.; Novoselov, K. S.; Geim, A. K. *Rev. Mod. Phys.* **2009**, *81*, 109.

(12) Thomsen, C.; Reich, S. *Phys. Rev. Lett.* **2000**, *85*, 5214.

(13) Duque, J. G.; Chen, H.; Swan, A. K.; Shreve, A. P.; Kilina, S.; Tretiak, S.; Tu, X.; Zheng, M.; Doorn, S. K. *ACS Nano* **2011**, *5*, 5233−5241.

(14) Shank, C.; Yen, R.; Fork, R.; Orenstein, J.; Baker, G. *Phys. Rev. Lett.* **1982**, *49*, 1660−1663.

(15) Zade, S.; Zamoshchik, N.; Bendikov, M. *Acc. Chem. Res.* **2011**, *44*, 14−24.

(16) Kramers, H. A.; Heisenberg, W. *Z. Physi. A Hadrons Nuclei* **1925**, *31*, 681−708.

(17) Lee, S.-Y. *J. Chem. Phys.* **1983**, *78*, 723−734.

(18) Martin, R. M., Falicov, L. M. Resonant Raman Scattering. In *Light Scattering in Solids I*; Springer: Berlin, 1983; *Vol. 8*, pp 79−145.

(19) Dirac, P. A. M. *Proc. R. Soc. London, Ser. A* **1927**, *114*, 243−265.

(20) Born, M.; Oppenheimer, R. *Ann. Phys.* **1927**, *389*, 457−484.

(21) Long, D. *Raman Spectroscopy*; McGraw-Hill: New York, 1977; pp 457−484.

(22) Heller, E.; Sundberg, R.; Tannor, D. *J. Phys. Chem.* **1982**, *86*, 1822−1833.

(23) Jumeau, D.; Lefrant, S.; Faulques, E.; Buisson, J. P. *J. Phys.* **1983**, *44*, 819−825.

(24) Schen, M.; Chien, J. C. W.; Perrin, E.; Lefrant, S.; Mulazzi, E. *J. Chem. Phys.* **1988**, *89*, 7615−7620.

(25) Schäfer-Siebert, D.; Budrowski, C.; Kuzmany, H.; Roth, S. *Synth. Met.* **1987**, *21*, 285−291.

DOI: 10.1021/acscentsci.5b00021
ACS Cent. Sci. 2015, 1, 40−49